BOR DERGİSİ
JOURNAL OF BORON
http://dergipark.gov.tr/boron

Effect of tungsten disilicide addition on tungsten boride based composites produced by milling-assisted pressureless sintering

Didem Ovalı*[1], Duygu Ağaoğulları[2], Hasan Gökçe[3], M. Lütfi Öveçoğlu[4]

[1]Istanbul Technical University, Metallurgical and Materials Engineering Department, Particulate Materials Laboratories (PML), 34469 Maslak, Istanbul, Turkey, ORCID ID orcd.org/0000-0002-7934-6535

[2]Istanbul Technical University, Metallurgical and Materials Engineering Department, Particulate Materials Laboratories (PML), 34469 Maslak, Istanbul, Turkey, ORCID ID orcd.org/0000-0002-0623-5586

[3]Istanbul Technical University, Prof.Dr. Adnan Tekin Materials Science and Production Technologies Applied Research Center, 34469 Maslak, Istanbul, Turkey, ORCID ID orcd.org/0000-0003-3672-4919

[4]Istanbul Technical University, Metallurgical and Materials Engineering Department, Particulate Materials Laboratories (PML), 34469 Maslak, Istanbul, Turkey, ORCID ID orcd.org/0000-0002-1536-4961

ARTICLE INFO

Article history:
Received 15 October 2017
Accepted 04 January 2018
Online 26 March 2018

Research Article

DOI: 10.30728/boron.344402

Keywords:
Tungsten boride,
Tungsten disilicide,
Milling,
Pressureless sintering,
Microhardness,
Oxidation stability

ABSTRACT

In this study, tungsten boride (WB and W_2B) based composites with various amounts of tungsten disilicide (WSi_2) addition were fabricated by using a combined method of mechanical milling (MM), cold isostatic pressing (CIP) and pressureless sintering (PS). MM was conducted for 4 h in ethanol (wet milling) and Argon atmosphere (dry milling) using a high-energy ball mill. WSi_2 was used with different amounts (0, 5, 10 and 20 wt.%) in order to investigate its effect on the resultant products. MM'd powders were compacted using CIP under a pressure of 450 MPa, and were consecutively sintered at 1600 °C for 2 h and 1770 °C for 2 h under Ar atmosphere. Compositional, physical and microstructural characterizations of the samples were performed using stereo and optical microscopes, X-ray diffractometer, TOPAS software, scanning electron microscope coupled with an energy-dispersive spectrometer, particle size analyzer and gas pycnometer. Sintered products were also characterized in terms of Archimedes density and Vickers microhardness. Moreover, the oxidation studies of the samples were performed at 500 and 1000 °C via thermogravimetric analyzer. The results showed that the highest density, microhardness and oxidation stability values amongst the fabricated composites were obtained for the dry milled and sintered WB-20 wt.% WSi_2 sample.

1. Introduction

High temperature structural ceramics such as borides, carbides, nitrides and silicides are good candidates for advanced applications thanks to their exceptional properties like high melting temperature, high hardness, high thermal conductivity and good corrosion resistance [1-3]. There are ample literature reported on the improvement of these ceramics in terms of densification, mechanical and physical properties, oxidation resistance and ablation resistance, by applying composite approaches[1,4-6] ZrB_2 and HfB_2 can be shown as examples of the most studied ceramic composites [4,5,7]. However, other borides can also be promising ceramics and worth investigating. Among transition metal borides, tungsten borides have potential usage for industrial applications at extreme environmental conditions. WB (2665 ºC) and W_2B (2670 ºC) are the most stable tungsten boride phases in the W-B binary phase diagram (containing WB, W_2B, W_2B_5, WB_4, WB_6 and WB_{12} phases) [8-10]. They exhibit interesting properties such as high melting points, high hardness values, high abrasion resistances, chemical inertness, magnetic and electrical properties and thermal shock resistances [10-13]. Furthermore, transition metal silicides are important materials due to their high temperature oxidation resistance and mechanical properties. Amongst them, tungsten disilicide (WSi_2) can be a good candidate as a reinforcement material thanks to its abrasive, adhesive wear and oxidation resistances [14,15]. In this manner, composites including boride and silicide phases may offer improved mechanical properties, oxidation and corrosion resistance, particularly at high temperatures [16-18]. As one kind of boride and silicide composite, WB-WSi_2 composites are promising as advanced structural materials. There are only few attempts for sintering of tungsten boride in the literature [19-22]. Grabis et al. fabricated WB_2 and B_4C composites by spark plasma synthesis from W_2C, C and amorphous B blends [20]. Kuzenkova et al. studied pressureless sintering of W_2B_5 at 1700 ºC and indicated that W_2B_5 phases decomposed into WB and B (which was further oxidized) phases [21]. In the study of Hamamoto et al., WB and W_2B_5 powders

*Correspondig author: didem.ovali@gmail.com

which contained amorphous B and different amounts of W powders were sintered by hot-pressing method [23]. In another study, ultrapure WB powders were hot-pressed at different pressure (1-3 GPa) and temperature (700-1000 ºC) values for 60 min, and high dense WB samples were produced [22]. Recently, Fan et al. reported a study on the theoretical assessments of WB phase and also some investigations on its physical and mechanical properties [24]. As a result of this study, they proposed the WB as a promising material for industrial applications as coatings, hard alloy tools and ceramics. However, there are no studies published about sintering of WB or WB based composites.

In the present study, the effect of WSi_2 addition (0, 5, 10 and 20 wt.%) was investigated on tungsten boride matrix for the first time, using mechanical milling, cold isostatic pressing and pressureless sintering methods. Sintered samples were characterized in regard of microstructure, density, microhardness and oxidation stability. This study will contribute to the archival literature and further investigations about tungsten boride based composites.

2. Materials and methods

2.1. Raw materials and powder preparation

In the experimental studies, commercial WB (Alfa Aaesar, -325 mesh, 99 % purity) and WSi_2 (Alfa Aaesar, -325 mesh, 99.5 % purity) powders were used. WSi_2 powders were added into the WB matrix with the amounts of 0, 5, 10 and 20 wt.%. Milling experiments were conducted in a Fritsch Pulverisette 5 planetary ball mill, and milling parameters were presented in Table 1. Milling performed in absolute ethanol (Merck) was referred as wet milling whereas milling carried out under Ar (Linde) atmosphere was referred as dry milling. After wet milling, powders were dried at 100 ºC for 12 h. Powders for dry milling experiments was handled in a Plaslabs glove box.

Table 1. Milling parameters.

Type of parameter	Value/Explanation
Speed	400 rpm
Capacity of vial	500 ml
Diameter of ball	10 mm
Vial and ball material	Yttria stabilized zirconia
Ball-to-powder weight ratio	20:1
Milling time	4 h
Milling atmosphere	Ar or absolute ethanol

2.2. Consolidation and sintering

Wet and dry milled powders were placed in silicon cylindrical molds having 6 mm diameter and height. Cold isostatic pressing (CIP) was applied to the molds under 450 MPa pressure. Compacted powders were sintered under Ar atmosphere in a Linn HT-1800 high-temperature controlled-atmosphere furnace according to the sintering regime given in Figure 1(a). For thermogravimetric analyses (TGA), powders were consolidated into cylindrical preforms with a diameter of 4 mm using a MSE cold press (CP) under a uniaxial pressure of 450 MPa. Specimens consolidated by CIP and CP were presented in Figure 1(b) and (c), respectively.

2.3. Characterization

Phase characterizations of the milled powders and sintered samples were performed using a Bruker D8 Advanced Series X-ray diffractometer (XRD) with CuK_α (1.54060 Å) radiation with 2θ value of 20-90º and step size of 2º/min. Bruker® Diffracplus EVA software was utilized to identify crystalline phases in the XRD patterns using the International Centre for Diffraction Database (ICDD) PDF-2 2016. Average crystallite sizes and lattice strains of the milled powders were calculated using TOPAS 4.2 (Bruker AXS) software [25]. Average particle sizes of the milled powders were

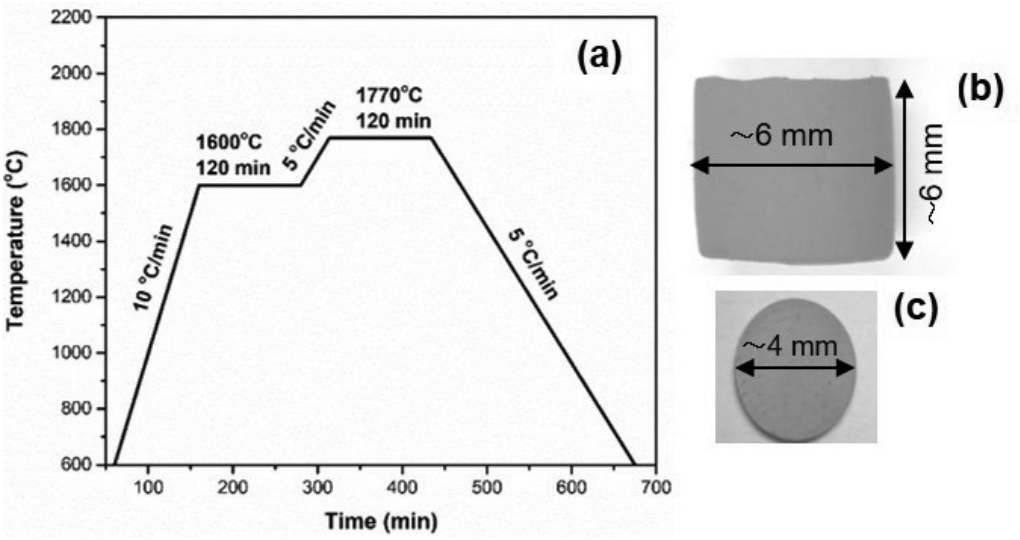

Figure 1. (a) Sintering regime, and SM images of the samples sintered by, (b) CIP, and (c) CP.

determined using a Microtrac Nano-flex particle size analyzer (PSA) equipped with a Bandelin Sonopuls ultrasonic homogenizer. Pycnometer densities of the milled powders were measured by a Micromeritics AccuPyc II 1340 gas pycnometer at room temperature using He gas (Linde) as the displacement medium.

General low-magnification images of the consolidated samples were taken using a Zeiss Discovery V12 stereomicroscope (SM) coupled with a Zeiss Axiocam ERc5s high resolution digital camera. Microstructural characterizations of the sintered samples were carried out using a Nikon Eclipse optical microscope (OM) and a Jeol-JCM-6000 benchtop (SEM) coupled with an energy-dispersive spectrometer (EDS). Densities of the sintered samples were determined using Archimedes method. Microhardness values of the sintered samples were obtained under the load of 200 g for 10 sec, and each sample included the mean value of 20 measurements and standard deviation. Moreover, the oxidation studies of the cold pressed and sintered samples were carried out at 500 and 1000 °C by TGA with heating rate of 10 °C/min and airflow of 200 ml/min.

3. Results and discussion

3.1. Characterization of the milled powders

Figure 2(a) and (b) show the XRD patterns of the 4 h of dry milled and wet milled WB-x wt.% WSi_2 (x=0, 5, 10 and 20) powders. There are only WB (ICDD card no: 73-1769, Bravais lattice: body-centered tetragonal, a=3.11 nm and c=16.93 nm) and WSi_2 (ICDD card no: 81-2168, Bravais lattice: body-centered tetragonal, a=3.21 nm and c=7.84 nm) phases. As expected, XRD intensity of the WSi_2 phase increased with its increasing amount. Comparing the XRD patterns of the dry and wet milled powders for the fixed WSi_2 amount, it can be clearly seen that the lack of ethanol in milling environment resulted in broader WB and WSi_2 peaks. Besides, the XRD intensities of the phases, especially WSi_2, are higher for the wet milled samples. This indicated higher amount of decrease in grain sizes at dry milling conditions in which high impact energy created by the effect of continuous collisions between balls, vial and particles. On the other hand, the presence of ethanol can limit the transfer of the impact energy to the powder particles. Furthermore, any formation of secondary phases and any contamination were not observed after dry and wet milling within the detection limit of the used diffractometer (> 2 wt.%).

Based on the XRD patterns in Figure 2(a) and (b), average crystallite sizes and lattice strains of the powders were determined taking into account the highest three peaks of the WB phase (reflections from (103), (105) and (112) planes at the 2θ values of 32.8, 39.3 and 42.48°). The average crystallite sizes and lattice strains of the WB phase in the milled powders are given in the Table 2. According to these results, the milling environments affected the crystallite size and strain values of the powders. Dry milled samples had smaller average crystallite size and higher lattice strain than those of wet milled ones. However, any significant difference was not observed in these values for both milling conditions as WSi_2 amount increased up to 20 wt.%. These findings are compatible with their XRD patterns. Moreover, average particle sizes of the dry milled powders were found around 350 nm whereas those of wet milled ones were around 500 nm (Table 2). These results showed that particle size was more effectively reduced in dry milling condition than that of wet milling for the studied ceramic system. A similar tendency was reported by Jung et al. for boron particles [26]. According to Table 2, pycnometer densities of the milled powders were about 10-20 % lower than their theoretical densities. The refinement of the particle sizes created vacancies and dislocations in the crystallite boundaries or subgrain boundaries [27]. This can be shown as the probable reason of the dif-

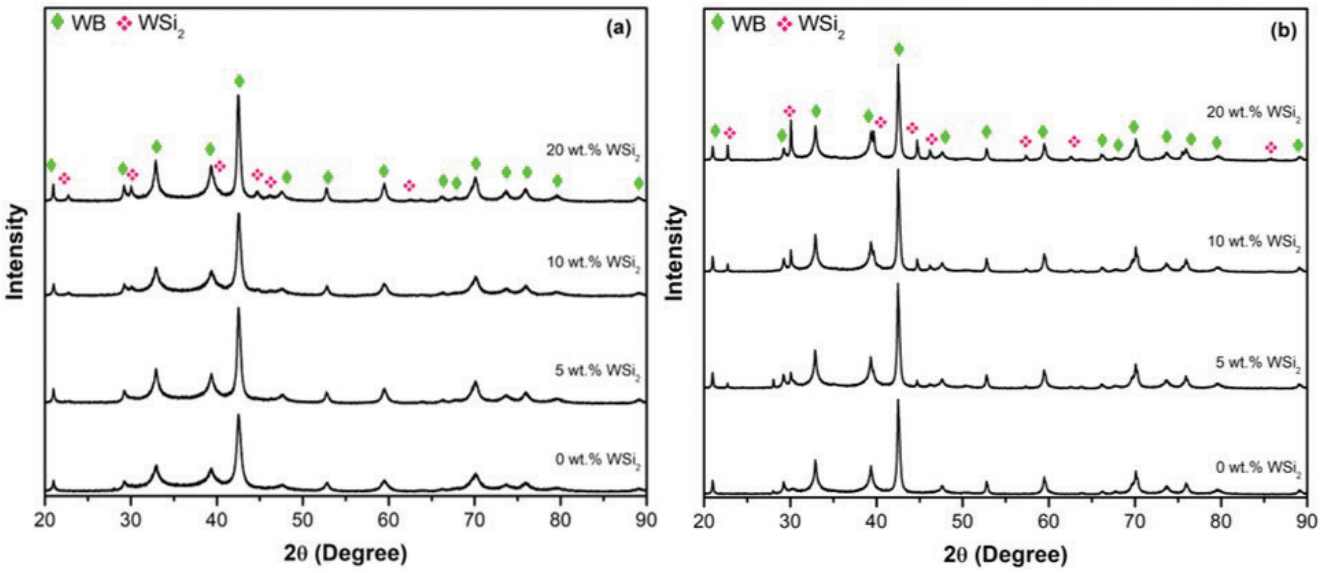

Figure 2. XRD patterns of the WB-x wt.% WSi_2 (x=0, 5, 10 and 20) powders after: (a) dry milling and (b) wet milling.

Table 2. Average crystallite sizes, lattice strains, particle sizes, theoretical and pycnometer densities of the dry and wet milled powders.

Parameters	Addition of WSi_2 (wt.%)							
	Dry Milling				Wet Milling			
	0	5	10	20	0	5	10	20
Crystallite Size (nm)	10.2	12.4	13.5	15.8	19.5	21.7	20.43	22.0
Lattice Strain	2.9	2.3	2.8	2.1	1.5	1.4	1.5	1.4
Average particle size D_{mean} (nm)	350±0.07	336±0.39	387±0.18	351±0.13	567±0.17	502±0.08	557±0.03	552±0.11
Theoretical density (g/cm^3)	15.3	15	14.7	14.1	15.3	15	14.7	14.1
Pycnometer density (g/cm^3)	13.9±0.01	13.2±0.02	12.5±0.01	12.04±0.01	13.03±0.01	12.66±0.02	12.04±0.02	11.72±0.04

ference between theoretical and pycnometer densities of the milled powders.

3.2. Characterization of the sintered products

Figure 3(a) and (b) illustrate the XRD patterns of the dry and wet milled, and sintered WB-x wt.% WSi_2 (x=0, 5, 10 and 20) samples. In these patterns, WB (ICDD card no: 73-1769, Bravais lattice: body-centered tetragonal, a=3.11 nm and c=16.93 nm), W_2B (ICDD card no: 025-0990, Bravais lattice: body-centered tetragonal, a=5.57 nm and c=4.74 nm) and WSi_2 (ICDD card no: 081-2168, Bravais lattice: body-centered tetragonal, a=3.21 nm and c=7.84 nm) were detected. Besides, the XRD patterns of the wet milled and sintered products (Figure 3(b)) revealed a very small amount of ZrO_2 phase (ICDD card no: 65-1024, Bravais lattice: primitive monoclinic, a=5.14 nm, b=5.21 nm and c=5.31 nm) arose from the wear of milling media. Similarly, there were some studies showing that wet milling caused more contamination than dry milling [26,28]. On the other hand, in another study about the milling media contamination, it was reported that yttria stabilized zirconia milling media provided the lowest contamination amongst hardened steel, tungsten carbide, partially stabilized zirconia, yttria stabilized zirconia and alumina vial and balls [29]. The W_2B phase was found as a dominant phase both in the XRD patterns of the wet and dry milled and sintered WB samples without WSi_2 addition. This means that some amount of WB has high affinity for transformation into the W_2B phase (lowest boride in the binary phase diagram) by the effect of sintering temperature. It was already reported that W_2B phase initiated at 1000 °C and its amount increased up to 1500 °C without any formation of other W borides [8,9]. Also, the formation of higher tungsten borides (WB, WB_4 and W_2B_5) were found favorable at temperatures below 1000 °C [9]. There should be some amount of B phase revealed during the formation of W_2B phase. However, any free B was not detected in the XRD patterns probably due to its non-crystalline structure or very small amount. The negative effect of amorphous B on the sintering of tungsten boride powders was previously reported [21]. Also, it can be said that wet milling promoted the formation of W_2B phase more than dry milling, based on the comparison of their peak intensities. According to Figure 3(a) and (b), it can comprehended that WSi_2 addition has a positive effect on the stability of WB phase. As the amount of WSi_2 increased from 0 to 20 wt.%, the peak intensities of W_2B phase decreased and those of WB phase increased. The dominant phase was WB for 20 wt.% WSi_2 added samples sintered from both dry and wet milled powders.

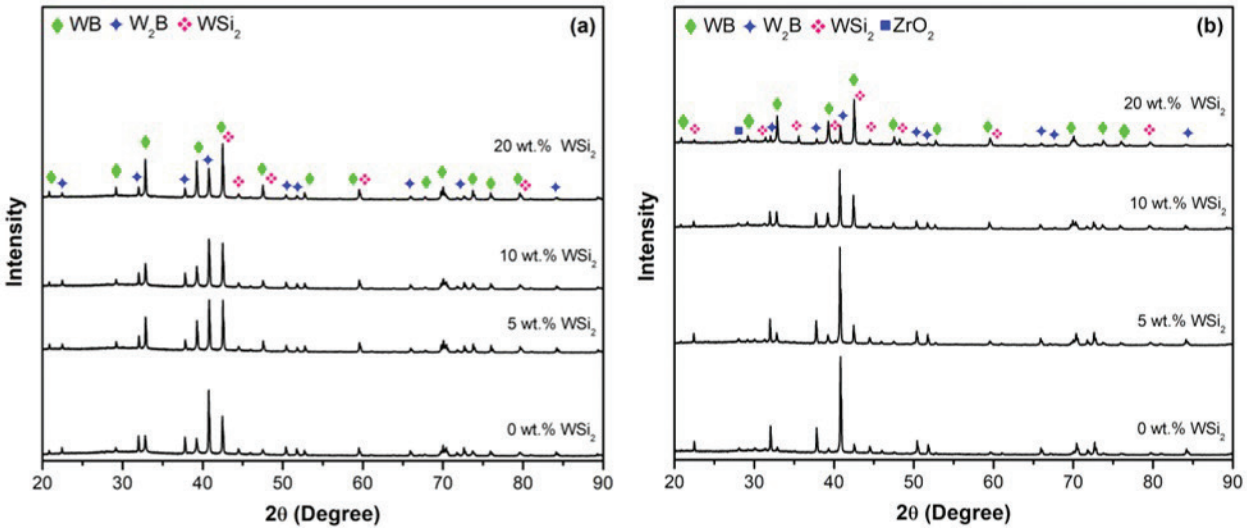

Figure 3. XRD patterns of the WB-x wt.% WSi_2 (x=0, 5, 10 and 20) bulk products sintered from the (a) dry milled powders and (b) wet milled powders.

OM images of the dry/wet milled and sintered products are demonstrated in Figure 4(a)-(h). Generally, it can be seen from the OM images that the phase distributions in the microstructure were improved by changing WSi_2 amounts. In the OM image of dry milled WB without any WSi_2 addition (Figure 4(a)), some segregations were observed in the microstructure. Increasing the amount of WSi_2 prevented the formation of these segregations and assisted to provide homogeneous distributions. (Figure 4(a)-(d)). In addition, the wet milled products (Figure 4(e)-(h)) had more homogeneous phase dispersion than those of dry milled ones (Figure 4(a)-(d)). Also, further WSi_2 addition reduced the particle sizes of the existing phases due to its brittle character for both milling conditions.

Green density of the compacted samples, Archimedes density and Vickers microhardness of the sintered products are given in Table 3. The green density values of the compacted samples increased approximately 15 % after sintering, indicating that the sintering process did not provide full densification. The Archimedes density and Vickers microhardness values of the products fluctuated according to the changing composition and milling atmosphere. There is no correlation between the increasing WSi_2 amount and property improvement, excepting 20 wt.% WSi_2 added samples. However, the Archimedes density and Vickers microhardness values of the products showed consistency with each other. The highest Archimedes density and Vickers microhardness values were belonged to the dry milled and sintered WB-20 wt.% WSi_2 sample. Even though the densities of dry milled and sintered WB-0 wt.% WSi_2 and WB-20 wt.% WSi_2 samples were similar, the addition of 20 wt.% WSi_2 resulted in a hardness difference about 4.55 GPa. Amongst the wet milled products, the highest density and microhardness were obtained in the WB-20 wt.% WSi_2 sample. However, the XRD patterns of the wet milled and sintered products pointed out the presence of ZrO_2 (Figure 3(b)). Existing undesired ZrO_2 contamination negatively affected the density values whose theoretical density values were calculated according to the WB and WSi_2 phases without taking into account the W_2B and ZrO_2 phases. In this content, the decrease in the density of dry milled products with increasing WSi_2 content

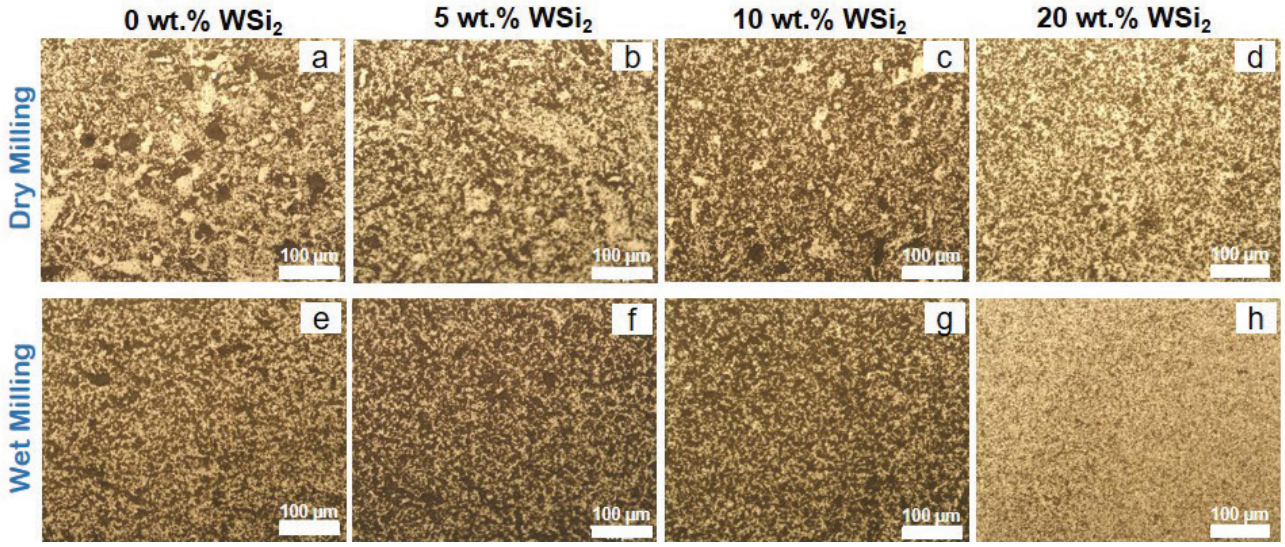

Figure 4. OM images of the WB-x wt.% WSi_2 bulk products sintered from the dry milled powders [(a) x=0, (b) x=5, (c) x=10, (d) x=20], and wet milled powders [(e) x=0, (f) x=5, (g) x=10, (h) x=20].

Table 3. Green density of compacted samples, and Archimedes density and Vickers microhardness of dry/wet milled and sintered WB-x wt.% WSi_2 (x=0, 5, 10 and 20) samples.

	Amount of WSi_2 (wt.%)	Green Density (%)	Archimedes Density (%)	Vickers Microhardness, (GPa)
Dry milling	0	67.2	90.5	8.85±2.4
	5	67.1	81.7	8.96±2.1
	10	70.3	83.8	8.34±1.9
	20	81.2	90.7	13.36±2.8
Wet milling	0	55.4	78.5	10.42±1.7
	5	57.9	80.5	6.78±1.9
	10	48.6	76.2	5.79±0.7
	20	62.6	86.9	11.54±2.7

could be related with the undetected ZrO_2. Chen et al. showed that the denseness of WB had an obvious effect on hardness, and fully dense WB product fabricated by an ultrahigh-pressure hot-press had an average hardness value of 28.9±0.8 GPa [30]. The different hardness values between the literature and this study can be attributed to the addition of WSi_2 phase, the formation of W_2B second phase, the emergence of ZrO_2 contamination and the lower density values of the sintered products caused by a different sintering method.

The SEM images taken from the fractured surfaces of the dry/wet milled and sintered products with the addition of 0, 10 and 20 wt.% WSi_2 are given in Figure 5(a)-(f). SEM micrographs showed that the addition of WSi_2 did not impair the densification mechanism of WB, in contrast with the Archimedes densities below 20 wt.% WSi_2 content (Table 3). According to SEM images, the average grain sizes were around 1-3 μm which indicated that a grain coarsening occurred during sintering. There were no significant change with increasing WSi_2 content in terms of grain size and morphologies of the sintered products. The presence of ZrO_2 contamination could not be detected from the fractured surfaces of the wet milled and sintered products. In order to detect the ZrO_2 contamination more clearly in the wet milled and sintered samples, SEM analyses were also conducted on the surfaces of the as-sintered samples. The representative SEM and EDS analyses of the wet milled and sintered WB-10 wt.% WSi_2 sample are illustrated in Figure 6(a) and (b), respectively. Figure 6(a) showed grains smaller than 5 μm. The EDS analysis of the red-marked region in Figure 6(a) pointed out that there was ZrO_2 contamination located between the grain boundaries. According to the general EDS result taken from whole sample surface, the detected amount of Zr was about 2 wt.%. However, Zr content in the red-marked area was determined as 58 wt.%. These results also indicated that the presence of ZrO_2 caused a low grain boundary diffusion rate and created a precipitation formation located at the grain boundaries which inhibited full densification [31].

3.3. Oxidation stabilities of the sintered products

In order to investigate oxidation stabilities of the composites, cold pressed and sintered samples were subjected to thermogravimetric analyses. Figure 7(a)-(d) indicates the weight change versus time plots of the dry/wet milled and sintered products during isothermal oxidation at 500 and 1000 ºC. It can be clearly stated that the addition of WSi_2 content had a positive effect on the oxidation behavior of WB. Continuous weight gain with time was observed at 500 ºC for all samples. Moreover, the weight gain got a similar rate with increasing WSi_2 content for both milling types in Figure 7(a) and (b). Wet milled samples exhibited slightly higher weight gaining at 500 ºC than those of dry milled samples. As obviously seen in Figure 7(c) and (d), dry milling contributed to the oxidation stabilities of the samples comparing to the wet milling at 1000 ºC. For this temperature, the weight gains suddenly accelerated after oxidation duration of 30 min and it slowed down after about 60 min. Although WB sample without WSi_2 addition showed the same oxidation curve for both milling types in Figure 7(c) and (d), the addition of WSi_2 content was found more effective for dry milling at 1000 °C, as similar to the behaviors at 500 °C. Thus, it can be said that the contribution of WSi_2 addition on the oxidation stability of WB was higher for dry milled samples at low and high temperatures than those of wet milled ones.

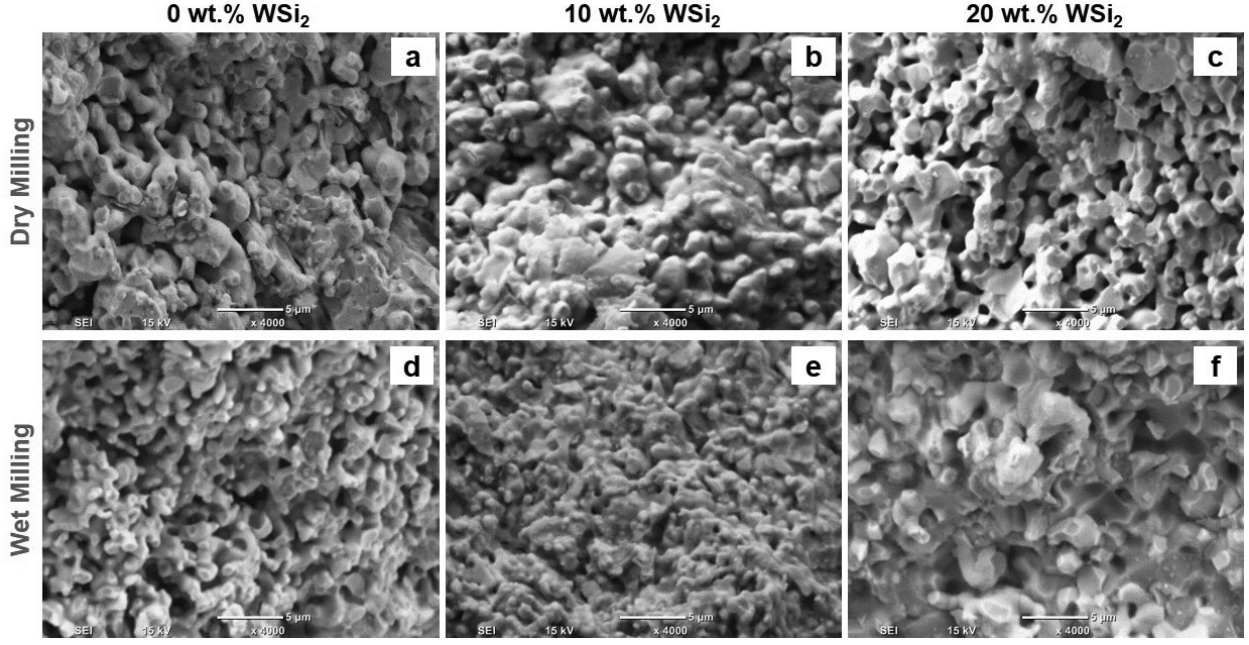

Figure 5. SEM images taken from fractured surfaces of the WB-x wt.% WSi_2 bulk products sintered from the dry milled powders [(a) x=0, (b) x=10 and (c) x=20] and wet milled powders [(d) x=0, (e) x=10 and (f) x=20].

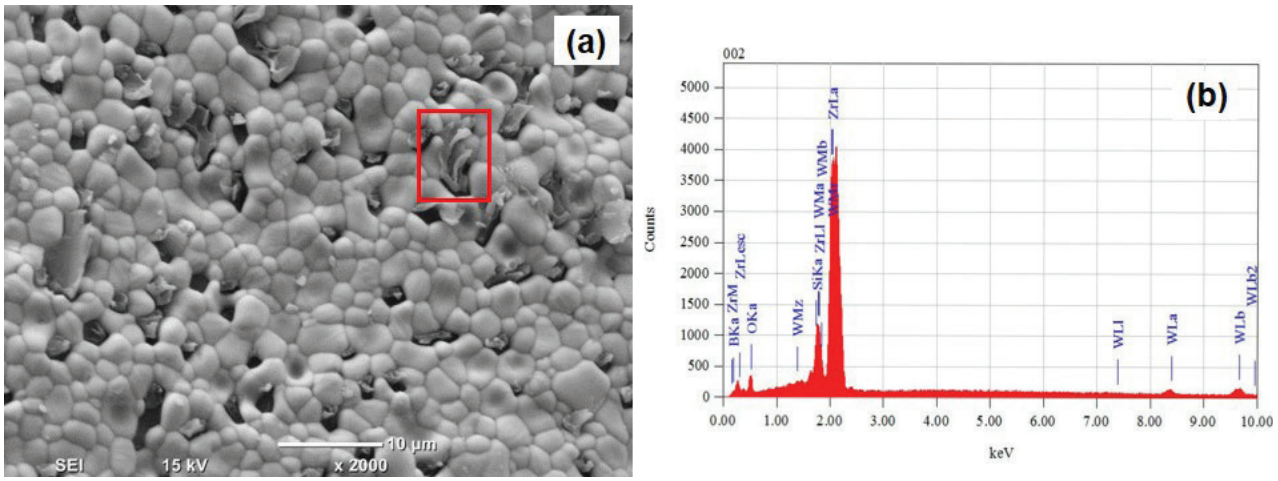

Figure 6. SEM/EDS analyses of the fractured surface of the wet milled and sintered WB-10 wt.% WSi_2 sample. (a) SEM image and (b) EDS analysis taken from the red-marked region in (a).

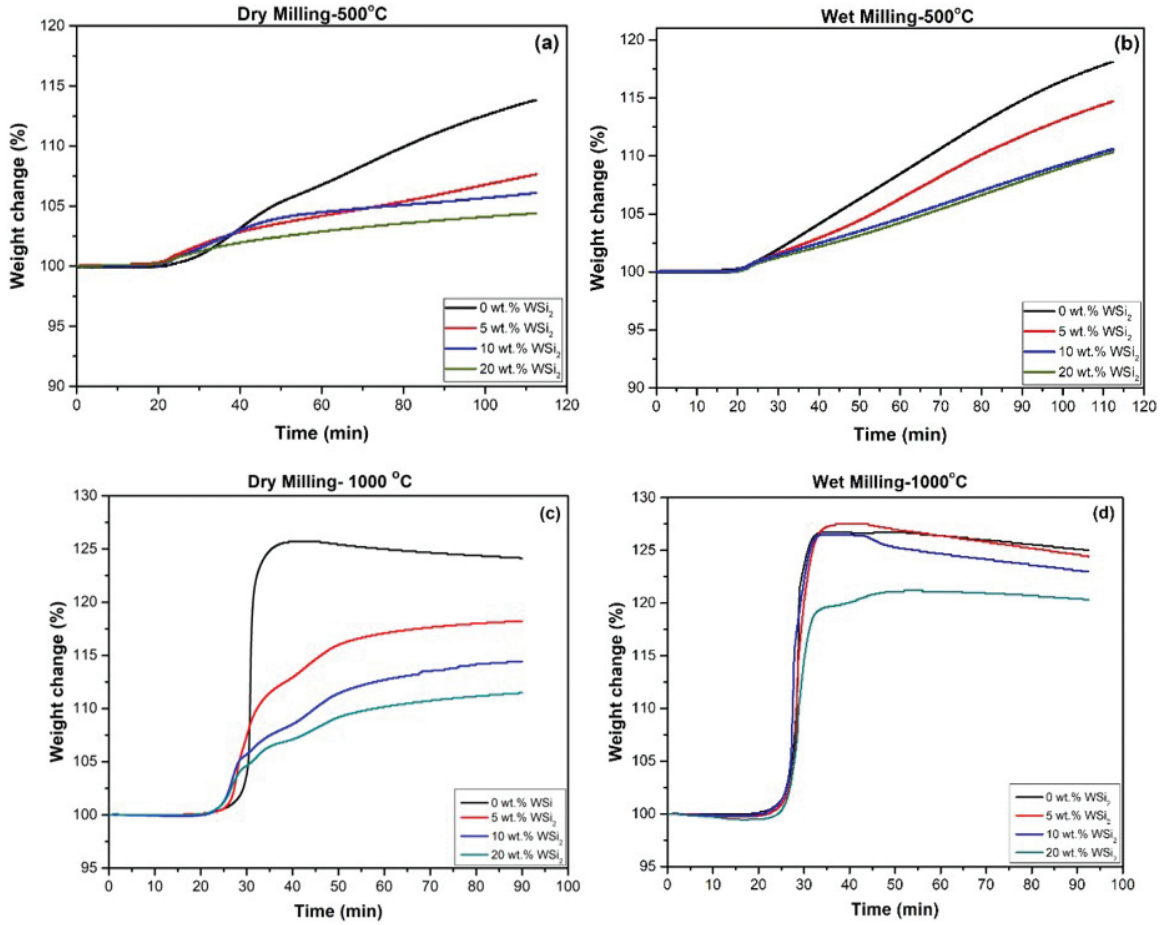

Figure 7. Weight change versus time plots of isothermal oxidation belonging to the WB-x wt.% WSi_2 (x=0, 5, 10 and 20) composites: (a) dry milled samples at 500 ºC, (b) wet milled samples at 500ºC, (c) dry milled samples at 1000 ºC and (d) wet milled samples at 1000 ºC.

Consequently, the addition of WSi_2 into the WB matrix improved the density and microhardness values after a particular amount whereas WSi_2 positively contributed to the oxidation behavior of tungsten borides for its all amounts. This study may lead for further investigations related with the transition metal borides, considering the improvements in the properties of tungsten borides.

4. Conclusion

In this study, WB-x wt.% WSi_2 (x=0, 5, 10 and 20) composites were fabricated by dry or wet milling, cold isostatic pressing and pressureless sintering. The sintered products consisted of WB, W_2B and WSi_2 phases. The XRD and SEM/EDS studies revealed that wet milled and sintered samples contained a small amount

of ZrO_2 contamination released from milling media. Although the density and microhardness values of the samples were not obtained as high as expected, they were in good correlation with each other. Oxidation tests showed that the addition of WSi_2 phase enhanced the oxidation stabilities of composites both under low and high temperatures. Comparing dry and wet milling processes prior to the sintering, it can be stated that their oxidation behaviors did not differ from each other at 500 ºC. However, dry milling was more effective in the oxidation stabilities of the composites at 1000 ºC**.** The best density (90.7 %), microhardness (13.36±2.8 GPa) and oxidation stability results amongst the fabricated composites were obtained for the dry milled and sintered WB-20 wt.% WSi_2 sample.

Acknowledgements

Authors would like to thank to Assist. Prof. Dr. Nuri Solak and Emin Kondakçı for their supports in cold isostatic pressing experiments.

References

[1] Weimer A. W., ed., Carbide, Nitride and Boride Materials Synthesis and Processing, 1st edition, Chapman & Hall, London, 1996.

[2] Ramberg C. E., Beatrice P., Kurokawa K., Worrell W. K., High temperature oxidation behavior of structural silicides, 21st Annual Cocoa Beach Conference And Exposition on Composites, Advanced Ceramics, Materials and Structures, 12-16 January, 1993.

[3] Suryanarayana C., Mechanical alloying and milling, Prog. Mater. Sci., 46, 1–184, 2001.

[4] Guo S. Q., Densification of ZrB_2-based composites and their mechanical and physical properties: A review, J. Eur. Ceram. Soc., 29, 995–1011, 2009.

[5] Murthy T. S. R. C., Sonber J. K., Sairam K., Bedse R. D., Chakarvartty J.K., Development of refractory and rare earth metal borides & carbides for high temperature applications, Mater. Today Proc., 3, 3104–3113, 2016.

[6] Kainer K. U., High temperature ceramic matrix composites, 1st edition, Wiley-VCH Verlag GmbH & Co. KGaA, Weinheim, 2006.

[7] Silvestroni L., Meriggi G., Sciti D., Oxidation behavior of ZrB_2 composites doped with various transition metal silicides, Corros. Sci., 83, 281–291, 2014.

[8] Predel B., B-W (Boron-Tungsten), B-Ba–C-Zr, Springer-Verlag, Berlin/Heidelberg, 1992.

[9] Itoh H., Matsudaira T., Naka S., Hamamoto H., Obayashi M., Formation process of tungsten borides by solid state reaction between tungsten and amorphous boron, J. Mater. Sci., 22, 2811–2815, 1987.

[10] Li Q., Zhou D., Zheng W., Ma Y., Chen C., Global structural optimization of tungsten borides, Phys. Rev. Lett., 110, 136-403, 2013.

[11] Kiessling R., The borides of some transition elements, J. Electrochem. Soc., 98 166–170, 1951.

[12] Brewer L., Sawyer D. L., Templeton D. H., Dauben C. H., A study of the refractory borides, J. Am. Ceram. Soc., 34 173–179, 1951.

[13] Barış M., Şimşek T., Gökmeşe H., Akkurt A., Characterization of W_2B nanocrystals synthesized by mechanochemical method, J. Boron., 1, 45–51, 2016.

[14] Petrovic J. J., High temperature structural silicides, 21st Annual Cocoa Beach Conference and Exposition on Composites, Advanced Ceramics, Materials and Structures, 12-16 January, 1993.

[15] Murthy T. S. R. C., Sonber J., Subramanian C., Hubli R., Suri A., Densification, characterization and oxidation studies of TiB_2–WSi_2 composite, Int. J. Refract. Met. Hard Mater., 33, 10–21, 2012.

[16] Silvestroni L., Sciti D., Balat-Pichelin M., Charpentier L., Zirconium carbide doped with tantalum silicide: microstructure, mechanical properties and high temperature oxidation, Mater. Chem. Phys., 143, 407–415, 2013.

[17] Sciti D., Bonnefont G., Fantozzi G., Silvestroni L., Spark plasma sintering of HfB_2 with low additions of silicides of molybdenum and tantalum, J. Eur. Ceram. Soc., 30, 3253–3258, 2010.

[18] Magnani G., Brentari A., Burresi E., Coglitore A., Mechanical properties and oxidation behavior of silicon carbide–molybdenum silicides composites, Ceram. Int., 39, 3345–3351, 2013.

[19] Cao X.-Z., Wang C., Xue X.-X., Yang H., Preparation of tungsten boride ceramic by pressureless sintering, J. Inorg. Mater., 29, 498–502, 2014..

[20] Grabis J., Šteins I., Sīpola I., Rašmane D., formation of high temperature compounds in W-C-B system by reactive spark plasma sintering, Mater. Sci., 21, 369–371, 2015.

[21] Kuzenkova M.A., Kayuk V.G., Kislyj P.S., Sintering of commercial tungsten boride produced by boron carbide method, Poroshk. Met., 10, 32–36, 1977.

[22] Chen Y., He D., Qin J., Kou Z., Wang S., Wang J., Ultrahigh-pressure densification of nanocrystalline WB ceramics, J. Mater. Res., 25, 637–640, 2010.

[23] Hamamoto H., Obayashi M., Matsudaira T., Itoh H., Naka S., Preparation of tungsten boride sintered compact by hot-pressing., J. Japan Soc. Powder Powder Metall., 35, 128–130, 1988.

[24] Fan C., Liu C., Peng F., Tan N., Tang M., Zhang Q., Wang Q., Li F., Wang J., Chen Y., Liang H., Guan S., Yang K., Liu J., Phase stability and incompressibility of tungsten boride (WB) researched by in-situ high pressure x-ray diffraction, Phys. B Condens. Matter., 521, 6–12, 2017.

[25] Jahangiri H., Öveçoğlu M.L., Determination of crystallite size, strain and solubility in mechanically alloyed W-xTi (x=0.5, 1.0, 4.0 and 10.0wt%) powder alloys, Mater. Lett., 178, 193–196, 2016.

[26] Jung H. J., Sohn Y., Sung H. G., Hyun H. S., Shin W. G., Physicochemical properties of ball milled boron particles: dry vs. wet ball milling process, Powder Technol., 269, 548–553, 2015.

[27] Zhang S., Khor K.A., Lü L., Preparation of Ti(C,N)-WC-TaC solid solution by mechanical alloying technique, J. Mater. Process. Tech., 48, 779–784, 1995.

[28] Ünal N., Öveçoğlu M. L., Effects of wet and dry milling conditions on properties of mechanically alloyed and sintered W–C and W–B_4C–C composites, Powder Metall., 52, 254–265, 2009.

[29] Reid C. B., Forrester J. S., Goodshaw H. J., Kisi E. H., Suaning G. J., A study in the mechanical milling of alumina powder, Ceram. Int., 34, 1551–1556, 2008.

[30] Chen Y., He D., Qin J., Kou Z., Bi Y., Ultrasonic and hardness measurements for ultrahigh pressure prepared WB ceramics, Int. J. Refract. Met. Hard Mater., 29, 329–331, 2011.

[31] Chamberlain A. L., Fahrenholtz W. G., Hilmas G. E., Pressureless sintering of zirconium diboride, J. Am. Ceram. Soc., 89, 450–456, 2006.